OPTIMIZED CALIBRATION CONSTANTS FOR THE CLEMENTINE NIR CAMERA. P. G. Lucey[1], D. T. Blewett[1,2], E. M. Eliason[3], L. A. Weller[3], R. Sucharski[3], E. Malaret[4], J. L. Hinrichs[1], P. D. Owensby[1,2]. [1]Planetary Geosciences/HIGP, Univ. of Hawaii, 2525 Correa Rd., Honolulu, HI 96822 (lucey@pgd.hawaii.edu); [2]Innovative Technical Solutions, Inc., 2800 Woodlawn Dr. #192, Honolulu, HI 96822; [3] U.S. Geological Survey, 2255 N. Gemini Dr., Flagstaff, AZ 86001;. [4] Applied Coherent Technology, Inc., 112 Elden St. #K, Herndon, VA 20170.

Introduction: The near-infrared (NIR) camera carried on the Clementine spacecraft obtained global imaging of the Moon in six wavelengths from 1.1 to 2.78 μm [1] . The major lunar rock-forming minerals plagioclase, pyroxene and olivine have diagnostic absorbtions in this wavelength range [e.g., 2], and hence the NIR dataset, in concert with data from Clementine's ultraviolet-visible (UVVIS) camera, has the potential to permit global mapping of lunar mineralogy and lithology. However scientific use of the NIR imagery has been hampered by a number of calibration problems [3, 4]. In particular, calibration constants previously reported resulted in large discontinuities in image mosaics straddling changes in camera state (gain, offset or integration time). We report here values of global constants which have been developed to minimize camera state discontinuities.

Global Optimization Strategy: Several efforts have been made to skirt the NIR calibration problems by performing an analysis for a restricted area and linking to telescopic spectra [5, 6]. Our aim is to determine the calibration constants globally to allow inter-comparison of all lunar areas. The objective here was to determine an optimum set of calibration constants which would minimize the difference between calibrated values for portions of the Moon imaged sequentially with different camera settings. To do this, we obtained statistics for all images collected during the systematic mapping phase of the mission that straddle camera-state boundaries. Approximately 19,800 cases were used in the analysis. At each state boundary, four overlapping images (in the same filter) were co-registered: two before the boundary and two following (Figure 1). The images had been corrected for pixel-dependent flat-field, dark and bias non-uniformities, then returned to raw digital number (DN) values. The average raw DN of each image overlap region was compiled in tabular form along with the frame number and camera state information. We denote these AB for the average value of the portion of image A that overlaps image B, BA for the average value of the portion of image B that overlaps image A, and so on. Hence at each boundary, we have three pairs of values: a pair before the boundary that were obtained with the first camera state setting (AB and BA), a pair straddling the boundary obtained at differing camera settings (BC and CB), and a pair following the boundary obtained at the second camera state setting (CD and DC). The before-boundary and after-boundary pairs serve as controls to insure that systematic drifts in camera values were not interpreted as global constant errors. The error function we sought to minimize was

$$| [2 \times (BC\text{-}CB)] - [(AB\text{-}BA) + (CD\text{-}DC)] |.$$

The optimization scheme is as follows. The calibration equation was applied to the entire set of data and the error function determined. Then a single calibration constant was incremented and decremented by a small fraction of its value (0.25%). The error function was recomputed using the "plus" and "minus" values, and the error function compared to the original. If the error function improved, the changed value of the constant was saved for use in the next iteration. If no change in the error function occurred, the starting value of the constant was retained for the next iteration. After each constant had been individually tested, all constants were updated to their new values and the process repeated. The optimization was run for a number of iterations until little change occurred in the error function. In this manner we simultaneously optimized the gain, exposure duration, digital offset, offset multiplier, and global bias. The offset mode ID itself is a pure digital value, and we considered it unlikely that it could actually vary from its assigned nominal value.

In the above discussion, the units for the "calibrated values" were gain-normalized counts per millisecond as computed from the calibration equation:

$$\text{Calib. Value} = \{([(DN\text{-}O_d)/G] - (O_{ID} \times V) - O_b)/t\} - C_d$$

Here DN is the raw DN, O_d is the digital offset, G is the gain, O_{ID} is the offset mode ID, V is the offset multiplier, O_b is the global bias, C_d is the mean dark current rate in counts/millisecond, and t is the exposure duration in milliseconds (refer to [4] for more details).

Results: We saw a large decrease in the value of the error function in the first 10-15 optimization iterations, followed by a much slower decline. The optimized values of the various constants settled near "final" values and we cut off the optimization after 45 steps. The optimized values of the global constants are: O_d = 8.3069, O_b = 2.15547, V = -0.95419. Our

method is insensitive to the value of the dark current so this value (which is indeterminate with respect to the thermal drift in the camera) is not reported. The optimized exposure duration and gain results are given in the Tables below. Two additional gain states used for high-latitude polar observations did not occur in our optimization data set, but we have calculated their gain values based on the switch settings in the gain circuit. They are: Gain ID Code 1, 28.2755; Gain ID Code 2, 24.9144.

Table 1. NIR Camera Exposure Durations, ms.

Nominal	11	33	57	95
Optimized	10.89	32.75	56.71	93.58

Table 2. NIR Optimized Gain Values.

Gain ID Code	Optimized Gain
42	6.16495
62	0.964975
61	1.40899
46	1.88595
31	2.43896
45	2.73995
23	3.48425
44	3.57405
53	4.08125
30	4.75472
52	5.39513
22	6.83130
29	6.95951
41	7.04438
13	7.77177

Image Tests: The statistical results of the optimization experiment indicated that major improvements were made in the matching of images across camera state boundaries. However the actual test is to examine calibrated images to determine if the boundaries disappear. Figure 2 presents a mosaic of images from Orbit 77 in the NIR E (2.6 μm) filter. The left image in Figure 2, calibrated with the nominal constants, shows a prominent discontinuity at a camera gain-state change. The marked improvement in the mosaic calibrated with the optimized gains demonstrates that the optimization has been successful.

Remaining Tasks: The calibrated values derived above still contain a large and variable instrumental background term. We are currently characterizing this offset. There are also four pixel-dependent non-uniformity fields which must be updated: dark current, bias, responsivity, and thermal background. For the last we have no existing estimate. Reasonable estimates exist for the first three and can be obtained from the authors.

References: [1] S. Nozette et al. (1994) *Science 266*, 1835-1839. [2] C. Pieters (1993) in *Remote Geochemical Analysis*, Cambridge Univ. Press, 309-339. [3] P. Lucey et al. (1997) *LPS XXVIII*, abstract #1401. [4] P. Lucey et al. (1998) *LPS XXIX*, abstract #1576. [5] A. McEwen et al. (1994) *Science 266*, 1858-1862. [6] S. Le Mouélic et al. (1999) *Geophys. Res. Lett. 26*, #9, 1195-1198; S. Le Mouélic et al. (1999) *J. Geophys. Res. 104*, #E2, 3833-3843.

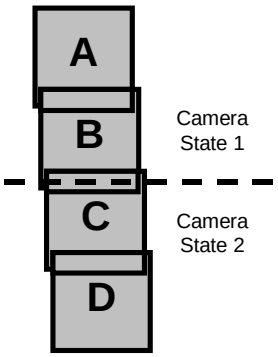

Figure 1. Illustration of image sets.

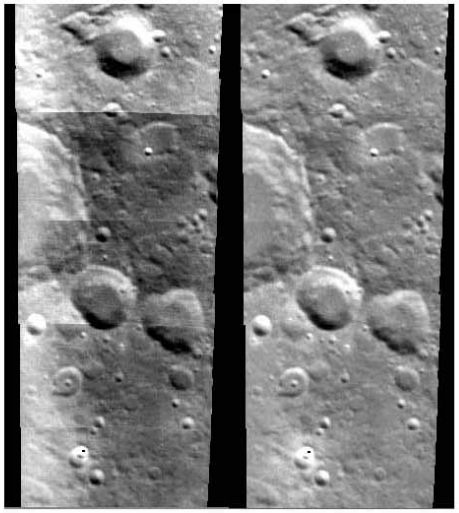

Figure 2. NIR filter E mosaics. *Left*: processed with nominal calibration constants. *Right*: processed with optimized constants. The image on the left has some center-to-edge shading caused by early versions of the flat field, and a discontinuity across a camera gain-state boundary is clearly visible. These problems are eliminated in the right image, processed with the optimized gains and updated flat-fields.